Influence of rough and smooth walls on macroscale granular segregation patterns

Umberto D'Ortona* and Nathalie Thomas
Aix-Marseille Université, CNRS, Centrale Marseille, M2P2 UMR 7340, 13451 Marseille, France

Richard M. Lueptow
Department of Mechanical Engineering, Northwestern University, Evanston, Illinois 60208, USA
(Received 14 October 2015; revised manuscript received 29 January 2016; published 26 February 2016)

Size bidisperse granular materials in a spherical tumbler segregate into two different patterns of three bands with either small particles at the equator and large particles at the poles or vice versa, depending upon the fill level in the tumbler. Here we use discrete element method simulations with supporting qualitative experiments to explore the effect of the tumbler wall roughness on the segregation pattern, modeling the tumbler walls as either a closely packed monolayer of fixed particles resulting in a rough wall or a frictional geometrically smooth wall. Even though the tumbler wall is in contact with the flowing layer only at its periphery, the impact of wall roughness is profound. Smooth walls tend toward a small-large-small (SLS) band pattern at the pole-equator-pole at all but the highest fill fractions; rough walls tend toward a large-small-large (LSL) band pattern at all but the lowest fill fractions. This comes about because smooth walls induce poleward axial drift of small particles and an equator-directed drift for large particles, resulting in an SLS band pattern. On the other hand, rough walls result in both sizes of particles moving poleward at the surface of the flow. Due to radial segregation, small particles percolate lower in the flowing layer and when arriving near the pole are caught in the return current drift that carries them back toward the equator incrementally with each passage through the flowing layer, while large particles remain at the surface near the pole, resulting in an LSL band pattern. The tendency toward either of the two segregation patterns depends on the fill level in the tumbler and the roughness of the tumbler's bounding wall.

DOI: 10.1103/PhysRevE.93.022906

I. INTRODUCTION

Discrete element method (DEM) simulations are used extensively to study the flow and segregation of granular materials in many situations as a predictive tool and to access data that are otherwise difficult to obtain experimentally. One of the key aspects of any simulation approach is the implementation of boundary conditions at walls. Two types of wall boundary conditions can be implemented in DEM simulations: (i) geometrically frictional smooth surfaces [1–5], which are assumed to have infinite mass and a specified radius of curvature (infinite for planar walls), and (ii) a geometrically rough surface made up of a closely packed monolayer of fixed particles conforming to the geometry of the wall surface (see, for example, [6–10]). However, a recent study of monodisperse flow in a spherical tumbler suggests that the results using the latter approach, often called a rough wall, differ from those using a smooth wall, not only locally at the particle scale but also globally across the entire flowing layer [11].

In this paper we explore the impact of rough and smooth walls on the axial segregation of size bidisperse spherical particles of equal density in a partially filled spherical tumbler rotating with angular velocity ω about the horizontal axis x, which passes through its center (Fig. 1), such that the free surface is essentially flat and continuously flowing. In this regime, the surface of the flowing layer maintains a dynamic angle of repose β with respect to the horizontal that depends on the frictional properties, the diameter d of the particles, and the rotational speed of the tumbler [12–15]. Due to the size difference between the particles, within 2–3 rotations radial segregation occurs with large particles at the free surface while small particles form a central core. In experiments with spherical tumblers approximately half filled with a 50%-50% size bidisperse mixture of particles and with smooth walls within 10–20 rotations, large particles accumulate near the poles of the tumbler with a band of small particles at the equator [16–18]. This pattern is inverted for lower fill fractions so that small particles accumulate near the poles with a band of large particles at the equator [17,18]. We note that multiple bands of small and large particles occur for bidisperse mixtures in long rotating cylindrical tumblers, which are used in applications for materials ranging from foodstuffs to mining to cement, typically after $O(10)$ to $O(100)$ rotations and having a wavelength of about one tumbler diameter [19] under a wide range of conditions [19–26]. In the cylindrical tumbler case, however, large particles segregate near the flat end walls of the tumbler [19,24,27], as a consequence of radial segregation combined with the nonuniform axial distribution of velocity in the flowing layer due to friction at the end wall [28]. This mechanism cannot occur in the spherical tumblers studied here.

Discrete element method simulations of spherical tumblers with smooth walls readily reproduce the segregation experiments in an acrylic spherical tumbler [17]. The mechanism for the inversion of the segregation bands from large-small-large (LSL) for higher fill fractions to small-large-small (SLS) at lower fill fractions remains unresolved, though a mechanism based on a difference in distance traveled down the flowing layer by large and small particles has been proposed [18]. In an initial effort to understand the segregation mechanism, we attempted further DEM simulations at different fill fractions

*umberto@l3m.univ-mrs.fr

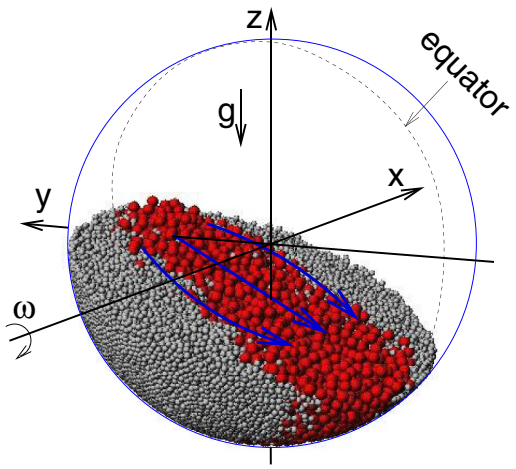

FIG. 1. A 14-cm-diameter spherical tumbler filled at 30% with 2- and 4-mm particles. The blue arrows at the free surface show the general direction of the flow. Here x is the polar axis and y and z are in the equatorial plane.

in spherical tumblers. However, to simplify the implementation of the simulations, we performed the simulations with rough wall boundary conditions. The results are dramatically different from the simulations with smooth frictional walls, as shown in Fig. 2. For otherwise identical systems (same particle sizes, rotational speed, tumbler diameter, and fill fraction), the surface segregation pattern changes from SLS for smooth walls [Fig. 2(a)] to LSL for rough walls made of 2-mm-diameter particles [Fig. 2(c)]. Using an intermediate wall particle size of 1.5 mm results in no significant surface band formation at all [Fig. 2(b)].

The unexpectedly strong influence of wall roughness on band formation led us to first study monodisperse flows in a spherical tumbler [11]. For monodisperse flows, the wall roughness strongly affects the particles trajectories, even far from walls. Particle trajectories at the free surface curve further toward the poles for smooth walls than for rough walls. However, the particle trajectories curve back toward the tumbler equator more in the smooth case as well, resulting in a smaller net poleward drift at the surface for smooth walls than for rough walls. The influences of the rotation speed and the fill level on trajectories were also considered. Increasing rotational speed increases the curvature of trajectories, but the drift is only slightly affected. The fill level has the opposite effect: An increase of the fill level decreases the curvature of the trajectories [11,17].

In this paper we examine through both DEM simulations and qualitative experiments the impact of wall boundary roughness on band formation in bidisperse flows. The effects of the fill level and the rotation speed are also studied numerically.

II. METHODS

A. Qualitative experiments

Since the different results for smooth and rough walls were initially obtained via DEM simulations, it was crucial to confirm that the predicted segregation patterns did in fact occur experimentally. Qualitative experiments were performed using clear acrylic spheres consisting of two mating hemispheres of

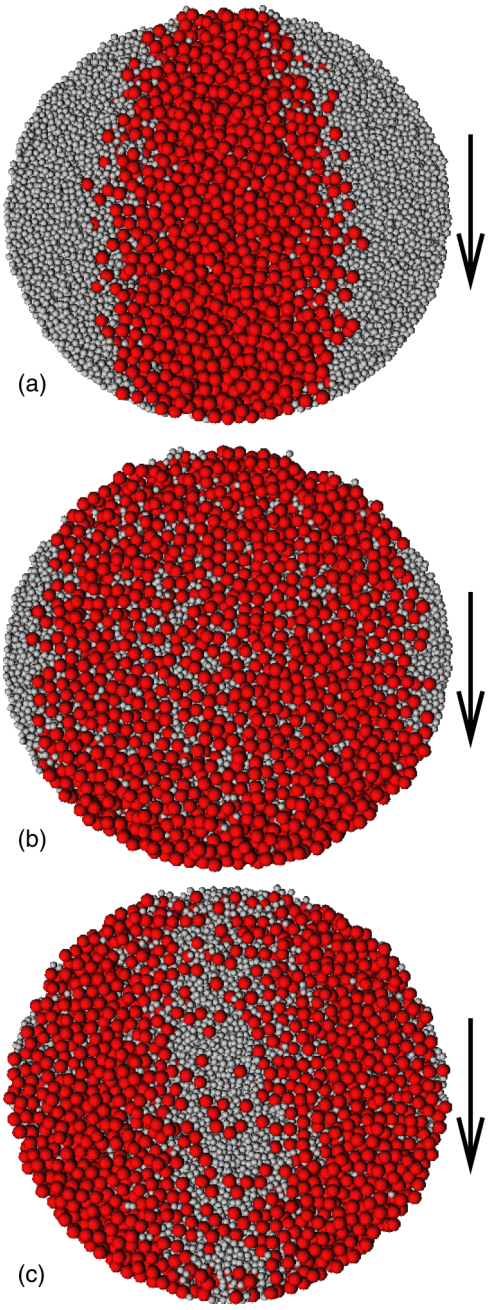

FIG. 2. Surface segregation patterns for equal volumes of 2- and 4-mm particles in a 30% full 14-cm-diameter spherical tumbler rotated at 15 rpm for $t = 200$ s. The tumbler walls are (a) smooth, (b) rough with 1.5-mm particles, and (c) rough with 2-mm particles. The rotation axis is horizontal and arrows show the direction of the surface flow.

diameter $D = 14$ cm rotated by an electric motor at 14.7 rpm about a horizontal axis. The tumbler was filled to 30% by volume with equal volumes of $d = 2$- and 4-mm-diameter spherical glass particles. For the rough wall case, the small particles were bonded to the wall of a tumbler using epoxy, thereby reducing the tumbler inner diameter to 13.6 cm. The tumbler was rotated for approximately 100 rotations and stopped so that all the particles were in one hemisphere. Then the upper hemisphere of the spherical tumbler was removed

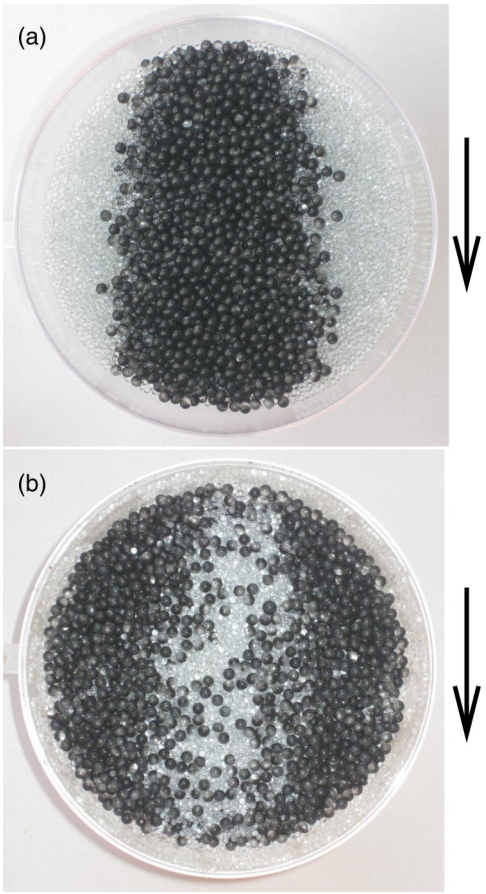

FIG. 3. Surface segregation patterns for equal volumes of 2-mm (transparent) and 4-mm (black) glass particles in a 30% full spherical acrylic tumbler rotated at 15 rpm for 400 s (100 rotations). The tumbler walls are (a) smooth and (b) rough with 2-mm particles. The rotation axis is horizontal and arrows show the general direction of the surface flow.

to obtain an image of the surface segregation pattern. The SLS segregation pattern occurs for the smooth tumbler wall [Fig. 3(a)], while the LSL segregation pattern occurs for the rough wall having 2-mm particles bonded to it [Fig. 3(b)], confirming the validity of the DEM results and the surprising effect of the wall roughness on the segregation pattern.

B. DEM simulations

For the DEM simulations, a standard linear-spring and viscous damper force model [29–32] was used to calculate the normal force between two contacting particles: $F_n^{ij} = [k_n\delta - 2\gamma_n m_{\rm eff}(\mathbf{V}_{ij}\cdot\hat{\mathbf{r}}_{ij})]\hat{\mathbf{r}}_{ij}$, where δ and $\mathbf{V}_{ij}$ are the particle overlap and the relative velocity $\mathbf{V}_i - \mathbf{V}_j$ of contacting particles i and j, respectively, $\hat{\mathbf{r}}_{ij}$ is the unit vector in the direction between particles i and j, $m_{\rm eff} = m_i m_j/(m_i + m_j)$ is the reduced mass of the two particles, $k_n = m_{\rm eff}[(\pi/\Delta t)^2 + \gamma_n^2]$ is the normal stiffness, and $\gamma_n = \ln e/\Delta t$ is the normal damping, with Δt the collision time and e the restitution coefficient [29,31]. A standard tangential force model [30,32] with elasticity was implemented: $F_{ij}^t = -\min(|\mu F_{ij}^n|, |k_s\zeta|)\mathrm{sgn}(\mathbf{V}_{ij}^s)$, where $\mathbf{V}_{ij}^s$ is the relative tangential velocity of two particles [4], k_s is the tangential stiffness, μ is the Coulomb friction coefficient, and $\zeta(t) = \int_{t_0}^{t}\mathbf{V}_{ij}^s(t')dt'$ is the net tangential displacement after contact is first established at time $t = t_0$. The velocity-Verlet algorithm [31,33] was used to update the position, orientation, and linear and angular velocity of each particle. Tumbler walls were modeled as both smooth surfaces (smooth walls) and as a monolayer of bonded particles of the same size (rough walls). Both wall conditions had infinite mass for calculation of the collision force between the tumbling particles and the wall.

The spherical tumbler of radius $R = 7$ cm was filled to volume fraction f with equal volumes of small and large particles of diameter 2 and 4 mm, except in some cases where 1- and 2-mm particles were used. The gravitational acceleration was $g = 9.81\ \mathrm{m\,s^{-2}}$. The particle properties corresponded to cellulose acetate: density $\rho = 1308\ \mathrm{kg\,m^{-3}}$ and restitution coefficient $e = 0.87$ [30,34,35]. The same restitution coefficient was used for walls made of particles and for smooth walls. The two species were initially randomly distributed in the tumbler with a total of about 5×10^4 particles in a typical simulation. To avoid a close-packed structure, the particles had a uniform size distribution ranging from $0.95d$ to $1.05d$. Unless otherwise indicated, the friction coefficients between particles and between particles and walls was set to $\mu = 0.7$ and the tumbler rotation speed was 15 rpm, resulting in a flat continuously flowing surface layer. The collision time was $\Delta t = 10^{-4}$ s, consistent with previous simulations [2,5,36] and sufficient for modeling hard spheres [31,37,38]. These parameters correspond to a stiffness coefficient $k_n = 7.32 \times 10^4\ \mathrm{N\,m^{-1}}$ [30], a Young modulus $E = 0.53$ GPa, and a damping coefficient $\gamma_n = 0.206\ \mathrm{kg\,s^{-1}}$. The integration time step was $\Delta t/50 = 2 \times 10^{-6}$ s to meet the requirement of numerical stability [31].

III. RESULTS

A. Segregation patterns

The steady-state concentration profiles corresponding to the experimental segregation patterns in Fig. 2 are shown in Fig. 4. A relative concentration of 1.0 corresponds to pure particles of one size. The profiles were obtained by determining the size of the particles intersecting a series of planes perpendicular to the axis of rotation (with $x = 0$ at the equator of the tumbler) and extracting the volume concentration for each species in that plane. This approach allows a much higher axial resolution for the concentration measurements than can be achieved with simple binning. For the SLS pattern in the smooth wall tumbler [Fig. 4(a)], the three bands are nearly pure (one particle size or the other for most of the width of each band). On the other hand, for the LSL pattern in the 2-mm rough wall tumbler [Fig. 4(c)], the bands are less pure and the transition between bands is not as sharp. The 1.5-mm rough wall [Fig. 4(b)] results in a configuration intermediate between the two other cases. The underlying reason for the nature of the concentration profiles is evident when viewing a cross section in a vertical plane and containing the axis of rotation (Fig. 5). For the SLS segregation pattern, the small particles and large particles form more distinct bands through the depth of the particle bed [Fig. 5(a)], while for the LSL surface pattern, the bands are much less sharp [Fig. 5(d)]. More interesting are the 1.0- and 1.5-mm rough wall cases [Figs. 5(b) and 5(c)]. In both cases, there is

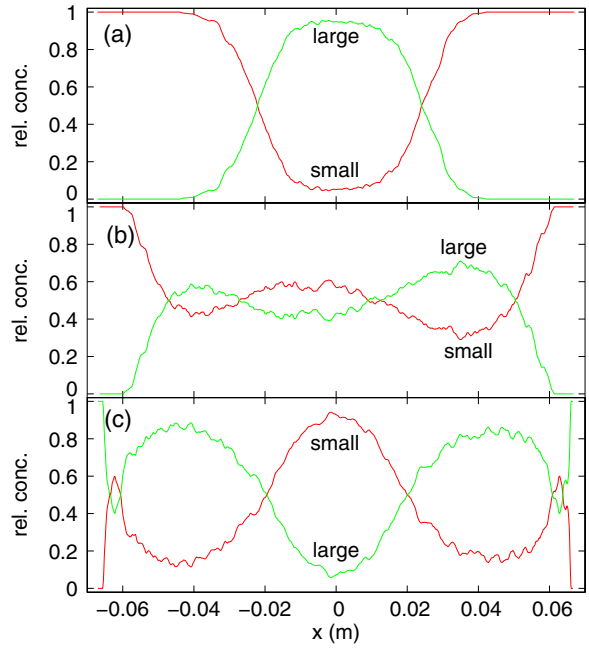

FIG. 4. Steady-state concentration profiles of small and large particles corresponding to Fig. 2: (a) smooth, (b) rough 1.5-mm particles, and (c) rough 2-mm particles.

a core of small particles across the entire width of the bed of particles with large particles surrounding the core. Figure 5(b) shows for 1-mm rough walls a configuration where the surface pattern is still SLS, but the band of large particles is less pure. In Fig. 5(c) particles have segregated radially but not axially, except right at the poles leading to no visible surface bands.

B. Axial segregation index

The segregation evolves over time from an initially well mixed state to a final segregated pattern. A convenient means to quantify the degree of segregation and its time evolution is an axial segregation index, defined as

$$I = \frac{1}{R}\left(\frac{\sum_{i=\text{large}} |x_i| v_i}{\sum_{i=\text{large}} v_i} - \frac{\sum_{i=\text{small}} |x_i| v_i}{\sum_{i=\text{small}} v_i}\right), \qquad (1)$$

where x_i is the position along the rotation axis with the equator at $x = 0$ (Fig. 1), v_i is the volume of the particle species i, R is the radius of the sphere, and the summations are over the large and small particles. The axial segregation index is positive for LSL and negative for SLS. The limit for perfect segregation is always less than one, but depends on the fill fraction. For a 50% full tumbler, perfect segregation would result in a segregation index of approximately ± 0.4 based on the tumbler's spherical shape.

Figure 6 shows the time evolution of the axial segregation index for the three wall roughness cases in Fig. 2 (with increasing wall roughness from top to bottom) for a range of fill fractions. Note that simulations were conducted until the segregation index reached its asymptotic value. Only the time evolution up to 400 s is presented here, but in some

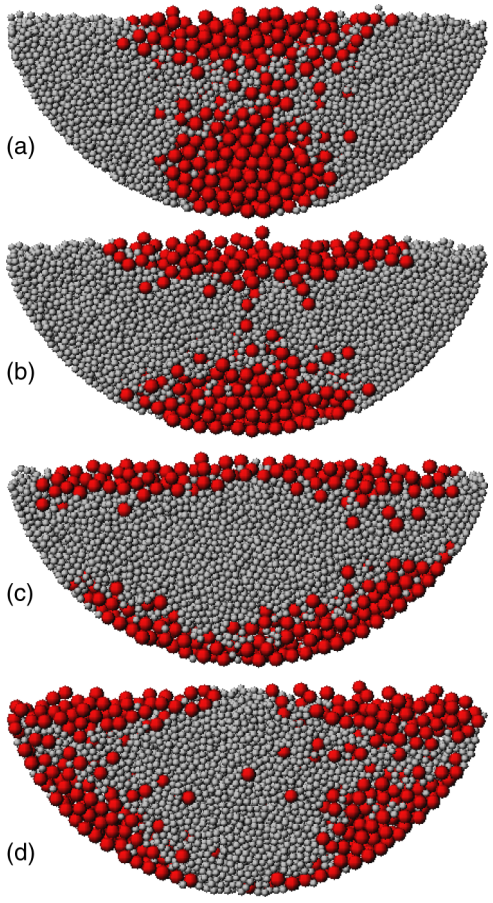

FIG. 5. Cross section of the segregation patterns in a vertical plane ($y = 0$) containing the axis of rotation corresponding to the surface patterns in Fig. 2 and concentration profiles in Fig. 4. The tumbler walls are (a) smooth, (b) rough with 1-mm particles, (c) rough with 1.5-mm particles, and (d) rough with 2-mm particles.

cases, simulations reached 1000 s. Regardless of the wall roughness, the segregation pattern is usually LSL ($I > 0$) for larger fill fractions and SLS ($I < 0$) for smaller fill fractions, consistent with experimental results for smooth walls [17,18]. Further note that LSL segregation ($I > 0$) is achieved more slowly than SLS segregation ($I < 0$) for a smooth wall, also consistent with experimental results [17]. However, this is to be expected because the time that particles spend in the flowing layer depends directly on the fill fraction. For low fill fractions, particles pass through the flowing layer more frequently than at high fill fractions for the same elapsed time [36]. Since only particles in the flowing layer have the opportunity to rearrange themselves (unlike particles below the flowing layer, which are locked into place in the bed of particles in solid body rotation), one could reasonably expect the segregation pattern to appear more quickly for low fill fractions than for high fill fractions. Similar results occur for rough walls.

The transition between LSL and SLS occurs at different fill fractions depending on the wall roughness (Fig. 7). The fill fraction for the transition decreases from 43% for the smooth wall case to 12% for the 4-mm rough wall case. At high fill fractions, the segregation gets close to nearly perfect LSL segregation, regardless of the wall roughness. Increasing the

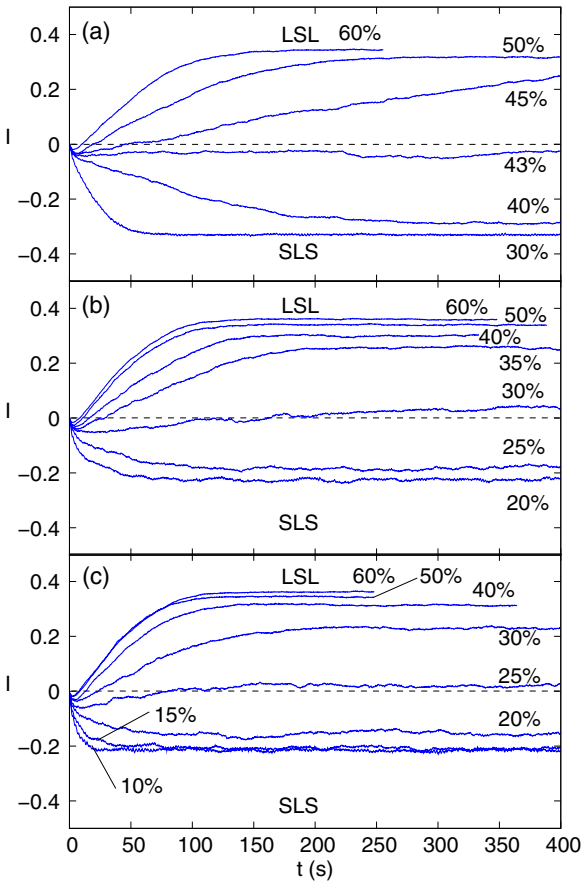

FIG. 6. Evolution of the axial segregation index I for equal volumes of 2- and 4-mm particles rotated at 15 rpm for several tumbler fill fractions (volume percentages indicated in the figure) and wall roughnesses: (a) smooth, (b) rough with 1.5-mm particles, and (c) rough with 2-mm particles.

wall roughness favors LSL segregation. At low fill fractions, the degree of SLS segregation depends on the roughness of the wall, with the smooth wall having the greatest segregation. However, the magnitude of the segregation index for SLS segregation is not as large as with LSL segregation, except for smooth walls. Note that fill fractions lower than those shown in Fig. 7 for roughnesses of 2 mm or less result in a

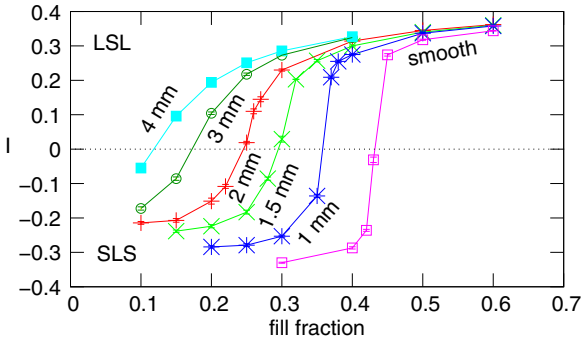

FIG. 7. Asymptotic value of the axial segregation index as a function of fill fraction for several wall roughnesses for equal volumes of 2- and 4-mm particles rotated at 15 rpm. Error bars (smaller than the symbols) are the standard deviation of the axial segregation index.

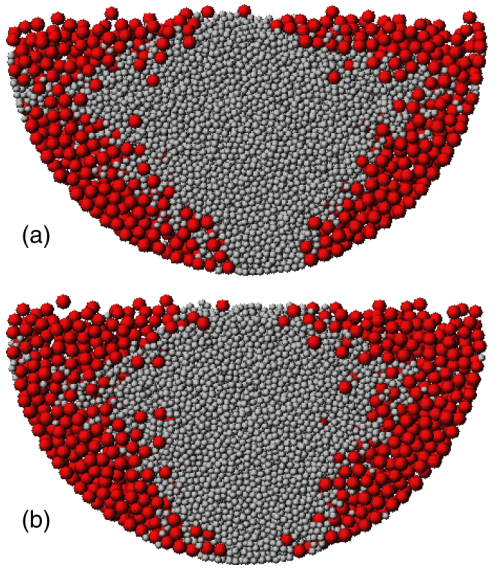

FIG. 8. Cross section of the segregation patterns in a vertical plane ($y = 0$) containing the axis of rotation (corresponding to a sphere filled at 50% with equal volumes of 2- and 4-mm particles). The tumbler walls are (a) smooth and (b) rough with 2-mm particles.

slip of the particle bed with respect to the tumbler, so they are not included in the figure. The transition from SLS to LSL at $I = 0$ is steepest for smooth walls.

It is helpful to consider the axial segregation index in Fig. 7 in the context of the segregation patterns in Fig. 5. Moving upward along a vertical line in Fig. 7 at a fill fraction of 30% starts with strong SLS segregation corresponding to Fig. 5(a) for a smooth wall. Increasing the wall roughness to 1-mm particles corresponds to the development of a core of small particles at the equator, shown in Fig. 5(b), reducing the axial segregation index, though the poles retain nearly pure small particles. For a 1.5-mm rough wall the segregation index is approximately zero, corresponding to a core of small particles surrounded by large particles extending nearly to the poles, shown in Fig. 5(c). A rougher wall of 2-mm particles corresponds to strong LSL segregation in which large particles dominate near the poles and small particles reach the flowing layer surface at the equator, shown in Fig. 5(d). This sequence is quite different from what occurs for a 50% fill level. There is almost no difference in the axial segregation index at a 50% fill level in Fig. 7 for different wall roughness values. The LSL segregation patterns shown in Fig. 8 at a 50% fill volume for smooth and 2-mm rough walls bear the similarity in the axial segregation index.

C. Particle trajectories

Previous results for the effect of wall roughness and fill level on particle trajectories in monodisperse flows provide some insights [11,36]. The trajectories in the flowing layer for both smooth and rough walls are curved. This curvature is negligible at the equator (at $x = 0$ cm, which is a plane of symmetry) and increases moving toward the pole. For particles near the surface of the flowing layer, the trajectory curvature for smooth walls is greater than that for rough walls. However,

the net poleward drift at the surface with each pass through the flowing layer for rough walls is larger than for smooth walls. Since surface particles drift poleward, particles deeper in the flowing layer drift toward the equator to conserve mass. As the fill level is reduced, the curvature of the particle trajectories increases for all roughnesses and the poleward drift decreases only for smooth walls but does not change significantly for rough walls.

These monodisperse results can be used to explain the bidisperse segregation patterns. Two effects compete to select the segregation pattern. First, particles are subject to a depth-dependent poleward drift. Since drift is larger at the surface [11], large particles that have segregated to the surface axially drift further poleward than small particles below the surface. Large particles remain at the surface due to radial segregation, so they accumulate near the poles. Small particles below the surface in the radially segregated core are transported by the global convection cells: from equator to pole nearer the surface and from pole to equator deeper in the flowing layer [36]. The second effect, which counteracts the drift, is the high curvature of the particle trajectories at the surface of the flowing layer, which is typical of smooth walls [11]. It results in both small and large particles being carried further poleward in the upstream portion of the flowing layer. Small particles tend to fall out of the flowing layer sooner than larger particles due to percolation, thus depositing in the fixed bed when they are closer to the poleward extrema of the trajectory than large particles, which tend to stay near the surface to curve back more toward the equator to deposit at an axial position near where they started. It is likely that for smooth walls, this trajectory curvature effect dominates, leading to the SLS pattern; for rough walls, where the trajectory curvature is smaller, the drift is very efficient and dominates [11], leading to the LSL pattern.

To confirm this mechanism, we plot pairs of trajectories for the two species of particles (2 and 4 mm) starting from the same initial positions in the flowing zone near the surface [specifically, when the center of a particle starts within a distance of 1 mm from a specified initial (x,y) coordinate that is 3 mm below the free surface], for tumblers with smooth or with 2-mm rough walls in Figs. 9 and 10. These trajectories are obtained by averaging thousands of individual particle trajectories starting from the same initial coordinate during the first few seconds (between $t = 2$ and 6 s) of the flow, before radial segregation is achieved. Like the monodisperse case [11], the trajectories in a tumbler with a smooth wall have a larger curvature than those for the rough case (Fig. 9). However, for the bidisperse case, large particles remain at the surface while small particles sink deeper into the flowing layer (Fig. 10), regardless of whether the walls are smooth or rough.

Consider now the trajectories in the smooth wall tumbler [Fig. 9(a)]. The trajectory curvature results in the large

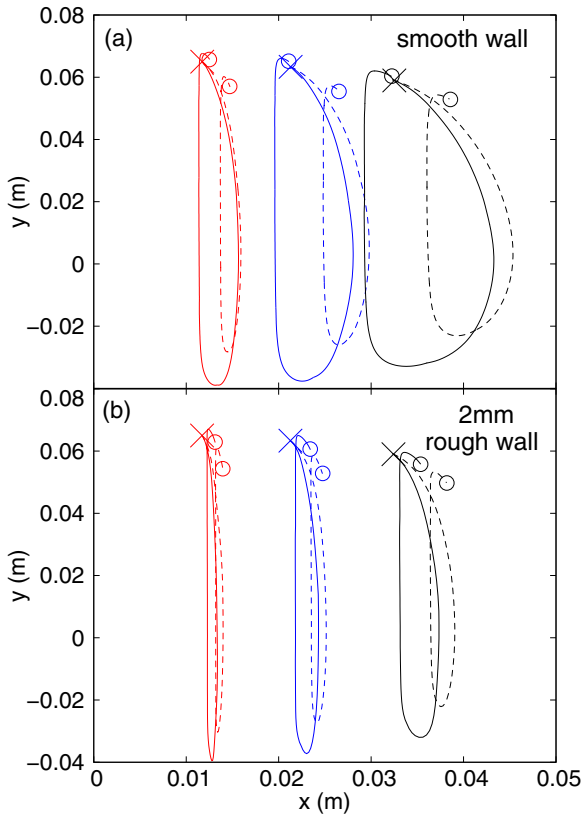

FIG. 9. Comparison (top view) of a pair of trajectories of 2-mm (dashed curves) and 4-mm (solid curves) particles starting from the same point (marked with an ×) in the flowing zone, at various x coordinates, in a tumbler made of (a) smooth walls or (b) rough 2-mm walls and filled at 30%. Circles show the end of each trajectory after one pass through the flowing layer and the fixed bed.

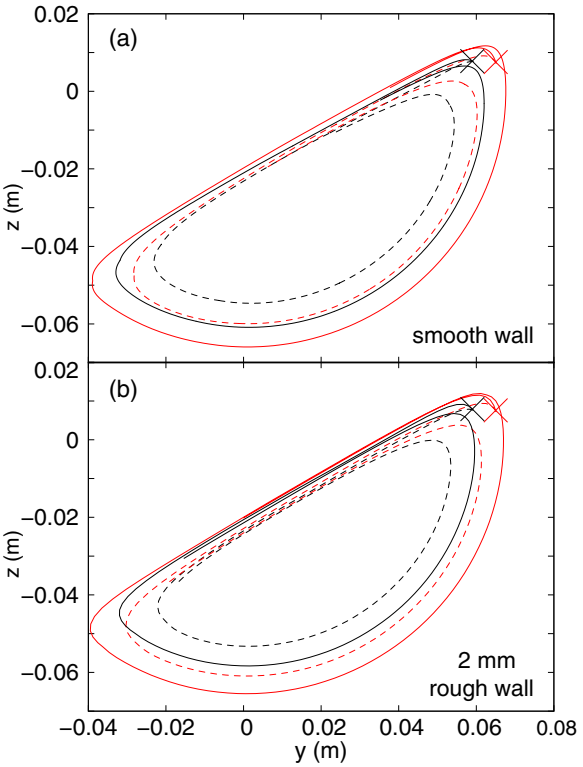

FIG. 10. Comparison (side view) of a pair of trajectories of 2-mm (dashed curves) and 4-mm (solid curves) particles starting from the same point (marked with an ×) in the flowing zone, but in various x positions, in a tumbler made of (a) smooth walls or (b) rough 2-mm walls and filled at 30%.

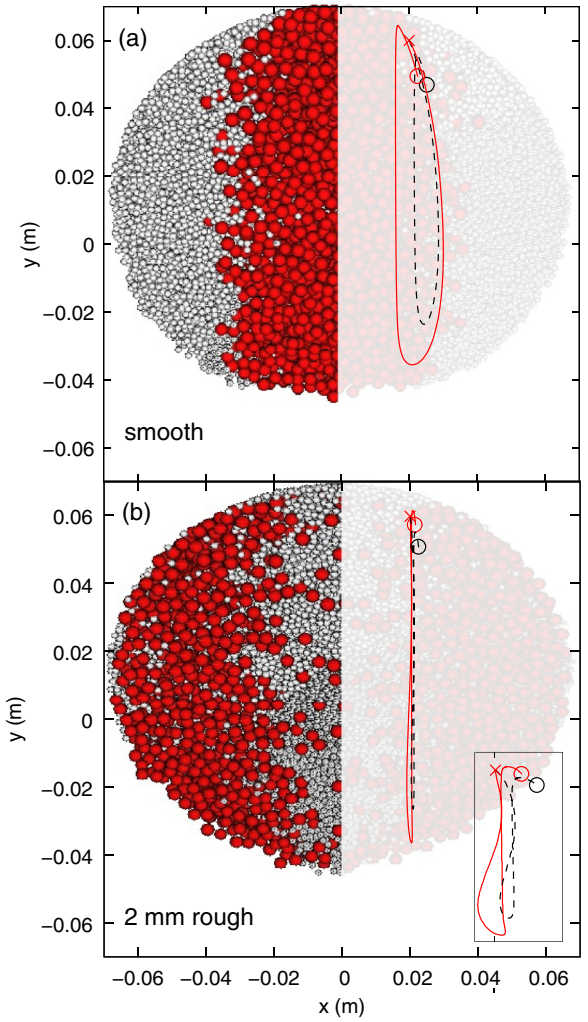

FIG. 11. Steady-state segregation pattern. Comparison (top view) of a pair of trajectories of 2-mm (dark gray dashed curves) and 4-mm particles (red solid curves) starting from the same point in the flowing zone (marked with an ×), at the border between the large and small particle regions, in a tumbler made of (a) a smooth wall or (b) rough 2-mm walls and filled at 30%. The surface of the flowing layer is at the angle of repose but viewed along the gravity vector, so its perimeter is oval. The inset in the bottom right of (b) shows the same trajectories reduced by a factor of 2 vertically and magnify by a factor of 10 horizontally. Circles show the end of each trajectory after one pass through the flowing layer and fixed bed.

particles, which stay near the surface, returning to a position very near where they started, while the small particles end up closer to the poles, regardless of their initial axial position. This difference in trajectories leads to the SLS segregation pattern, which dominates for smooth walls. The process is quite rapid and thus is always dominant in the first moments of the flow (even for rough walls). This is evident in Fig. 6, where the segregation indices in all cases are negative during the few first seconds, even in the cases of asymptotic LSL segregated systems. Also note that fully developed segregation is reached more quickly for SLS than for LSL (also observed experimentally [17]).

On the other hand, for rough walls, the curvature of the trajectories for both small and large particles is less, but the net drift of both particles is toward the pole [Fig. 9(b)]. Due to the radial segregation, large particles stay at the surface, whereas small particles are deeper in the flowing layer. When particles arrive at the pole, large particles remain at the surface, while small particles below the surface tend to drift back toward the equator slightly with each passage through the flowing layer much like they do in the monodisperse case [11,36]. The drift effect tends toward an LSL segregation pattern and dominates when the trajectory curvature is small.

Analogous results occur when varying the fill level. At low fill levels, particle trajectories are more curved [11], which favors SLS segregation. At high fill levels, trajectories are nearly straight [11], so the axial drift, as the particles segregate to different depths, dominates, leading to the LSL segregation pattern.

At the steady state for either SLS or LSL patterns, the particle trajectories appear to stabilize each pattern. This is shown in Fig. 11, where we compare the trajectories of large and small particles by plotting pairs of trajectories for the two particle species at the boundary between the large and small particles. In the case of smooth walls, the trajectories for the small and large particles diverge substantially even after only one pass through the flowing layer, resulting in displacement toward the pole for small particles and displacement toward the equator for large particles, reinforcing the SLS pattern.

This is not the case for the LSL segregation pattern for rough walls where displacements are very small and are toward the pole [see the inset of Fig. 11(b)]. Both species have nearly the same axial position after one pass through the flowing layer. The axial segregation occurs indirectly as a result of the radial segregation in the flowing layer, which keeps large particles near the surface. Consequently, the return flow toward the equator deep in the flowing layer consists of only small particles. Thus only small particles reach the surface near the equator where the core current emerges. The consequence is a very sharp boundary at the surface between small and large particles for the SLS segregation pattern and a more diffuse boundary for the LSL case (see Fig. 11). These differences are also evident in the experimental results in Fig. 3 and [17].

D. Wall friction and roughness

A question that naturally arises is if wall Coulomb friction could play a role similar to wall roughness in the evolution of segregation patterns based on the implicit assumption that a rough wall should have an effect similar to a high coefficient of friction for a smooth wall. To consider this, we use a higher coefficient of friction for wall-particle interactions than for particle-particle interactions in simulations for smooth walls. As shown in Fig. 12, the segregation evolution for a wall coefficient of friction of 1.5 is nearly identical to that for a wall coefficient of friction of 0.7, which is the particle-particle coefficient of friction. Of course, increasing the coefficient of friction too much results in a nonphysical situation in which slip will not occur at all. Hence, it is difficult to explain the differences between smooth and rough walls based on the argument that Coulomb friction is equivalent to wall roughness, at least within the constraints of the simulations.

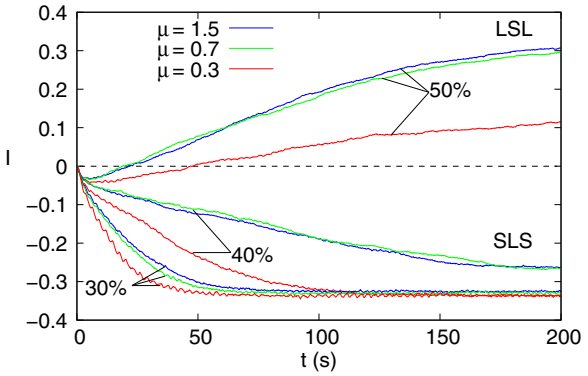

FIG. 12. Evolution of the axial segregation index for 2- and 4-mm particles rotated at 15 rpm for smooth walls but having wall coefficients of friction of $\mu = 0.3$, 0.7, and 1.5 for fill fractions of 30%, 40%, and 50%, respectively.

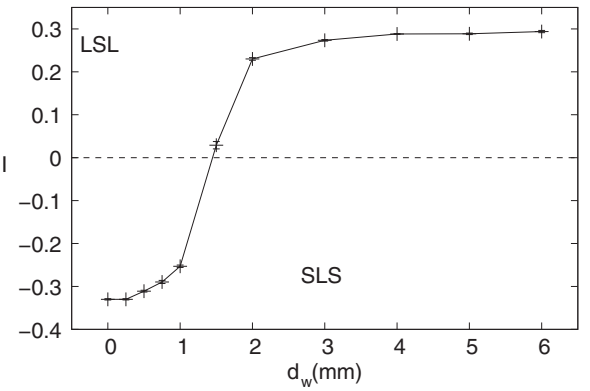

FIG. 14. Asymptotic value of the axial segregation index as a function of the roughness of the wall for 2- and 4-mm particles at 30% fill. Error bars (smaller than the symbols) are the standard deviation of the axial segregation index.

Another interesting situation is where the wall-particle friction coefficient is decreased to a low value compared to the particle-particle friction coefficient, shown in Fig. 12 for a wall coefficient of friction of 0.3. For all fill levels, the axial segregation index is lower. Indeed, with a lower wall friction coefficient, particles flow more easily along the wall, so the trajectories are more curved, favoring the SLS segregation pattern. For the 30% fill level case, the friction coefficient is low enough to be very close to a slumping regime, evident as the small oscillations of the segregation index.

Next we consider the effect of variation of the roughness of the wall. The evolution of the axial segregation index for the different wall roughnesses and a fill level of 30% is shown in Fig. 13. As observed previously (Figs. 6 and 7), the segregation index increases with wall roughness. When the roughness is much larger than the size of the flowing particles, there is little influence on the axial segregation index. This is likely because the smaller flowing particles fill the gaps between the larger wall particles, which alters particle trajectories [11]. However, when the wall particles are smaller than the flowing particles, small changes can have significant impact. This is even more evident when considering the asymptotic value of the segregation index, shown in Fig. 14. The greatest impact on the segregation index for a mixture of 2- and 4-mm particles occurs when the wall particle size is between 1 and 2 mm.

It is also interesting to note that the perfectly smooth frictional wall, modeled as a spherical smooth surface with infinite mass, behaves similarly to a rough wall of 0.25-mm particles, suggesting that modeling a wall as fixed particles can be effective so long as the wall particles are much smaller than the flowing particles and the wall has the same coefficient of friction as the particles.

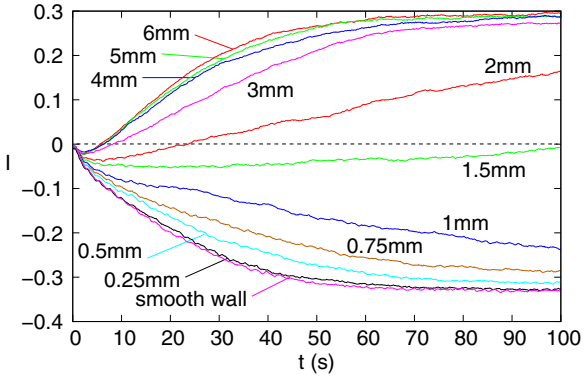

FIG. 13. Comparison of the time evolution of the axial segregation index for 2- and 4-mm particles at 30% fill and different wall roughnesses.

E. Tumbler rotational speed

A rotation speed of 15 rpm was selected for most simulations as a compromise to have fast simulations while maintaining a flat flowing layer. Nevertheless, varying the rotation speed can reverse the segregation pattern from LSL to SLS in experiments for the case of a tumbler with a smooth wall at a fill level of 50% [17].

To consider the impact of rotation speed, Fig. 15 shows the evolution of the axial segregation index for the smooth wall and 1.5-mm rough wall cases at rotation speeds of 5–30 rpm and a 30% fill level. Increasing rotation speeds reduces the

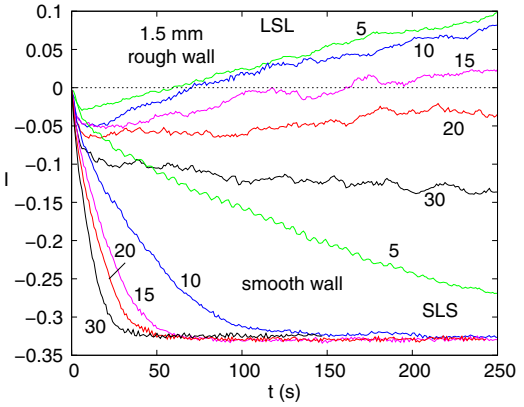

FIG. 15. Time evolution of the axial segregation index for 2- and 4-mm particles at 30% fill for a 1.5-mm rough wall (upper curves) and a smooth wall (lower curves) at rotation speeds $\omega = 5$, 10, 15, 20, and 30 rpm.

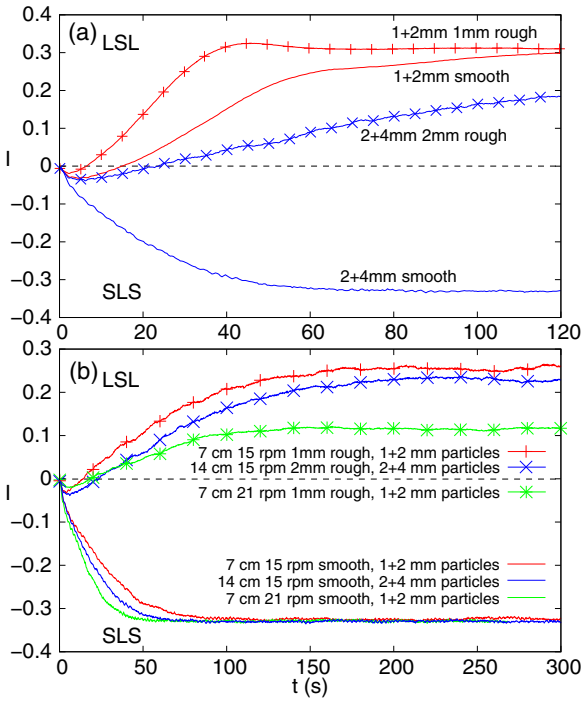

FIG. 16. (a) Comparison of the axial segregation index for a (1+2)-mm (red) and (2+4)-mm (blue) system in a 14-cm tumbler filled at 30%. (b) Two homothetic systems (at the same rotation speed or same Froude number): (1+2)-mm particles in 7-cm tumblers and (2+4)-mm particles in 14-cm tumblers filled at 30%.

segregation index. For the 1.5-mm rough wall case, a change from the LSL to the SLS segregation pattern occurs with increasing rotation speed just as is the trend observed in experiments for a smooth wall and a 50% fill level [17]. This phenomenon is likely related to the dependence of the particle mean trajectories on the rotation speed [11]. When the rotation speed increases, the curvature of the particle trajectories increases while the drift toward the pole is almost unaffected. Since curvature of the trajectories promotes the SLS segregation pattern while a strong drift is associated with the LSL pattern, an increase of the rotation speed favors the SLS pattern. The trend toward a change from SLS to LSL with decreasing rotational speed for smooth walls is clearly evident in Fig. 15 for a 30% fill level, consistent with experimental results for a 50% fill level with smooth walls [17].

F. Size ratio

To further consider the relative size effects of the tumbler and particles, we performed a limited number of simulations with 1- and 2-mm particles in a 14-cm tumbler with both smooth and 1-mm rough walls. Because many more particles are simulated in this situation than with 2- and 4-mm particles, only low fill levels (30%) and shorter runs were feasible. The results in Fig. 16(a) demonstrate that relative particle and tumbler sizes make a difference for both smooth and rough walls. The decrease in particle size induces an increase in the axial segregation index. For example, in the smooth wall case, the 1- and 2-mm particles form an LSL pattern, while 2- and 4-mm particles form an SLS pattern, consistent with experimental results [17,18]. This is because the particle trajectory curvature increases with particle size, but net axial drift remains almost independent of particles size [11], and large curvature trajectories favor SLS segregation. With the trajectory curvature being smaller for small particles, a (1+2)-mm particle system will adopt the LSL segregation pattern more easily than a (2+4)-mm system, as is observed experimentally [17] and shown in Fig. 16(a).

Consider now a 7-cm tumbler (30% full) in which the entire system (particle sizes, wall roughness, and tumbler diameter) is scaled to half the size of the previous simulations, compared to a 30% full (2+4)-mm system at the same rotation speed. The differences between the large and small systems are relatively small as shown in Fig. 16(b). Results for the same Froude number $\mathrm{Fr} = \omega^2 R/g$ for the 7-cm tumbler at 21 rpm and the 14-cm tumbler 15 rpm are also shown in Fig. 16(b). For now, we simply note that conserving the rotation speed while reducing the system size results in similar axial segregation index curves, while conserving the Froude number results in different degrees of axial segregation for different system sizes. Changing the drum size suggests that the key mechanism is probably the differences in the trajectories for large and small particles.

IV. CONCLUSION

Bidisperse particle segregation in a spherical tumbler provides an ideal test for evaluating the impact of wall boundary conditions because of its sensitivity to the wall roughness and easily visualized results. It is clear that surface boundary conditions have a strong influence on the flow and subsequent segregation patterns. The bands form due to a combination of curved particle trajectories and the axial drift in the flowing layer. While the roughness of the walls determines the curvature and drift, these quantities along with radial size segregation determine the nature of the axial segregation pattern. For adequate fill levels, smooth walls result in more-curved trajectories with little drift and consequently SLS patterns; rough walls result in less-curved trajectories with more drift and consequently LSL patterns. At large fill levels, the axial LSL patterns always occur regardless of wall roughness. At lower fill levels, axial SLS patterns are more likely to occur.

Many questions remain including why the curvature and drift are so dependent upon the size of the system and rotation speed. Nevertheless, the nonlocality of granular flow (wall roughness modifies the trajectories and band formation far from the wall) is evident, as is the case in many other situations for granular pattern formation.

[1] M. Moakher, T. Shinbrot, and F. J. Muzzio, Powder Technol. **109**, 58 (2000).

[2] P. Chen, J. M. Ottino, and R. M. Lueptow, New J. Phys. **13**, 055021 (2011).

[3] N. Taberlet, W. Losert, and P. Richard, Europhys. Lett. **68**, 522 (2004).
[4] D. C. Rapaport, Phys. Rev. E **65**, 061306 (2002).
[5] N. Taberlet, M. Newey, P. Richard, and W. Losert, J. Stat. Mech. (2006) P07013.
[6] F. da Cruz, S. Emam, M. Prochnow, J.-N. Roux, and F. Chevoir, Phys. Rev. E **72**, 021309 (2005).
[7] J. J. McCarthy and J. M. Ottino, Powder Technol. **97**, 91 (1998).
[8] T. Pöschel and V. Buchholtz, Chaos Soliton. Fract. **5**, 1901 (1995).
[9] G. Juarez, P. Chen, and R. M. Lueptow, New J. Phys. **13**, 053055 (2011).
[10] F. Bertrand, L. A. Leclaire, and G. Levecque, Chem. Eng. Sci. **60**, 2517 (2005).
[11] U. D'Ortona, N. Thomas, Z. Zaman, and R. M. Lueptow, Phys. Rev. E **92**, 062202 (2015).
[12] N. Taberlet, P. Richard, A. Valance, W. Losert, J. M. Pasini, J. T. Jenkins, and R. Delannay, Phys. Rev. Lett. **91**, 264301 (2003).
[13] S. W. Meier, R. M. Lueptow, and J. M. Ottino, Adv. Phys. **56**, 757 (2007).
[14] S. Courrech du Pont, P. Gondret, B. Perrin, and M. Rabaud, Europhys. Lett. **61**, 492 (2003).
[15] F. Pignatel, C. Asselin, L. Krieger, I. C. Christov, J. M. Ottino, and R. M. Lueptow, Phys. Rev. E **86**, 011304 (2012).
[16] J. F. Gilchrist and J. M. Ottino, Phys. Rev. E **68**, 061303 (2003).
[17] P. Chen, B. J. Lochman, J. M. Ottino, and R. M. Lueptow, Phys. Rev. Lett. **102**, 148001 (2009).
[18] L. Naji and R. Stannarius, Phys. Rev. E **79**, 031307 (2009).
[19] G. Juarez, J. M. Ottino, and R. M. Lueptow, Phys. Rev. E **78**, 031306 (2008).
[20] Y. Oyama, Bull. Inst. Phys. Chem. Res. (Tokyo) **18**, 600 (1939).
[21] M. B. Donald and B. Roseman, Brit. Chem. Eng. **7**, 749 (1962).
[22] M. Nakagawa, Chem. Eng. Sci. **49**, 2540 (1994).
[23] O. Zik, D. Levine, S. G. Lipson, S. Shtrikman, and J. Stavans, Phys. Rev. Lett. **73**, 644 (1994).
[24] K. M. Hill and J. Kakalios, Phys. Rev. E **49**, R3610 (1994).
[25] K. M. Hill and J. Kakalios, Phys. Rev. E **52**, 4393 (1995).
[26] N. Jain, D. V. Khakhar, R. M. Lueptow, and J. M. Ottino, Phys. Rev. Lett. **86**, 3771 (2001).
[27] S. J. Fiedor and J. M. Ottino, Phys. Rev. Lett. **91**, 244301 (2003).
[28] P. Chen, J. M. Ottino, and R. M. Lueptow, Phys. Rev. Lett. **104**, 188002 (2010).
[29] P. Chen, J. M. Ottino, and R. M. Lueptow, Phys. Rev. E **78**, 021303 (2008).
[30] J. Schäfer, S. Dippel, and D. E. Wolf, J. Phys. (France) I **6**, 5 (1996).
[31] G. H. Ristow, *Pattern Formation in Granular Materials* (Springer, Berlin, 2000).
[32] P. A. Cundall and O. D. L. Strack, Geotechnique **29**, 47 (1979).
[33] M. P. Allen and D. J. Tildesley, *Computer Simulation of Liquids* (Oxford University Press, New York, 2002).
[34] T. G. Drake and R. L. Shreve, J. Rheol. **30**, 981 (1986).
[35] S. F. Foerster, M. Y. Louge, H. Chang, and K. Allia, Phys. Fluids **6**, 1108 (1994).
[36] Z. Zaman, U. D'Ortona, P. B. Umbanhowar, J. M. Ottino, and R. M. Lueptow, Phys. Rev. E **88**, 012208 (2013).
[37] C. S. Campbell, J. Fluid Mech. **465**, 261 (2002).
[38] L. E. Silbert, G. S. Grest, R. Brewster, and A. J. Levine, Phys. Rev. Lett. **99**, 068002 (2007).